Received: 4 February 2021 | Revised: 14 May 2021 | Accepted: 26 May 2021

DOI: 10.1002/mp.15036

MEDICAL PHYSICS

TECHNICAL NOTE

# Technical Note: Four-dimensional deformable digital phantom for MRI sequence development

**Hanna M. Hanson**[1] | **Björn Eiben**[2] | **Jamie R. McClelland**[2] | **Marcel van Herk**[1] | **Benjamin C. Rowland**[1]

[1]Division of Cancer Sciences, Faculty of Biology, Medicine and Health, The University of Manchester, The Christie NHS Foundation Trust, Manchester, UK

[2]Centre for Medical Image Computing, Radiotherapy Image Computing Group, Department of Medical Physics and Biomedical Engineering University College London, London, UK

**Correspondence**
Hanna Maria Hanson. Department 58, The Christie NHS Foundation Trust, Wilmslow Road, Manchester, M20 4BX, UK.
Email: hanna.hanson@postgrad.manchester.ac.uk

**Funding information**
Engineering and Physical Sciences Research Council, Grant/Award Number: EP/R5131631/1; NIHR Manchester Biomedical Research Centre; Cancer Research UK, Grant/Award Number: A21993

## Abstract

**Purpose:** MR-guided radiotherapy has different requirements for the images than diagnostic radiology, thus requiring development of novel imaging sequences. MRI simulation is an excellent tool for optimizing these new sequences; however, currently available software does not provide all the necessary features. In this paper, we present a digital framework for testing MRI sequences that incorporates anatomical structure, respiratory motion, and realistic presentation of MR physics.

**Methods:** The extended Cardiac-Torso (XCAT) software was used to create $T_1$, $T_2$, and proton density maps that formed the anatomical structure of the phantom. Respiratory motion model was based on the XCAT deformation vector fields, modified to create a motion model driven by a respiration signal. MRI simulation was carried out with JEMRIS, an open source Bloch simulator. We developed an extension for JEMRIS, which calculates the motion of each spin independently, allowing for deformable motion.

**Results:** The performance of the framework was demonstrated through simulating the acquisition of a two-dimensional (2D) cine and demonstrating expected motion ghosts from $T_2$ weighted spin echo acquisitions with different respiratory patterns. All simulations were consistent with behavior previously described in literature. Simulations with deformable motion were not more time consuming than with rigid motion.

**Conclusions:** We present a deformable four-dimensional (4D) digital phantom framework for MR sequence development. The framework incorporates anatomical structure, realistic breathing patterns, deformable motion, and Bloch simulation to achieve accurate simulation of MRI. This method is particularly relevant for testing novel imaging sequences for the purpose of MR-guided radiotherapy in lungs and abdomen.

**KEYWORDS**
digital phantom, motion management, MRI guidance, MRI simulation

## 1 | INTRODUCTION

Lung cancer remains one of the most common types of cancer, with 2 million people worldwide receiving the diagnosis in 2018.[1] The recently developed MR-linac for radiotherapy not only offers new treatment opportunities for lung cancer patients,[2,3] but also presents new challenges requiring novel imaging approaches.

Currently, a treatment fraction on MR-linac can last up to an hour,[2,3] compared to 10–15 min when treated on a conventional linac. Patients spend most of this time in an uncomfortable treatment position, resulting in fatigue or even the need to stop the treatment in the middle of a fraction.[3] To make the treatment easier to tolerate, the overall time must be reduced considerably, which includes reducing the scan time. For this reason, optimizing MR sequences for the task of image-guided radiotherapy is important. Spatial accuracy is an important consideration for radiotherapy, as the images are used to plan the treatment, align the plan to the patient anatomy at the start of a fraction and track the tumor position during delivery. Due to the presence of organs that are extremely sensitive to radiation, dose shifts as small as 1 mm can lead to worse patient outcomes.[4,5] Additionally low proton density in the lungs and respiratory motion can also affect image quality and introduce artifacts.

A number of methods are available for testing and optimizing novel MRI sequences. Patients or healthy volunteers can be scanned; however, there is no way of knowing what the true anatomy looked like during imaging. Two subsequent scans are not always directly comparable due to shifts and deformations in internal organ position in part caused by respiratory motion. Physical phantoms solve both of those problems, but most phantoms only feature simple one-dimensional movement and lack anatomical structure. MR simulation offers an alternative method for testing new sequences during development. The gold standard for MR simulation is Bloch simulation, which is based on numerical solutions to the Bloch equations. These simulators require extensive computational power, but can simulate more aspects of MR physics than analytical models. A number of different implementations exist;[6-8] some of these can simulate rigid motion, however none incorporate deformable motion. Rigid motion is suitable for simulating some scenarios, such as the patient moving their head during a brain scan; however, respiratory motion is more complex and involves deformations in addition to displacements. Thus there is currently no way to perform Bloch simulations of lung MR with realistic presentation of artifacts that arise from respiratory motion.

Therefore, there is a need for a digital phantom for MR simulation, that is anatomically accurate, incorporates realistic breathing patterns, and allows deformable motion. In this project, we describe the creation of a new digital phantom framework combining the Extended Cardiac Torso Phantom[9] (XCAT) digital human model with a version of the JEMRIS[6] Bloch simulator modified to support deformable motion. This work is an extension of a previous conference publication,[10] with a more efficient and realistic motion model, a detailed description of the implementation and additional experiments.

## 2 | MATERIALS AND METHODS

### 2.1 | XCAT

A schematic of the framework is provided in Figure 1. The first stage incorporates the XCAT software, which was designed for creating four-dimensional (4D) anthropomorphic phantoms for imaging research. It is based on the visible male and female anatomical datasets from the National Library of Medicine, which have been segmented and turned into nonuniform rational B-spline and subdivision surfaces. To generate an instance of the XCAT phantom, the software modifies

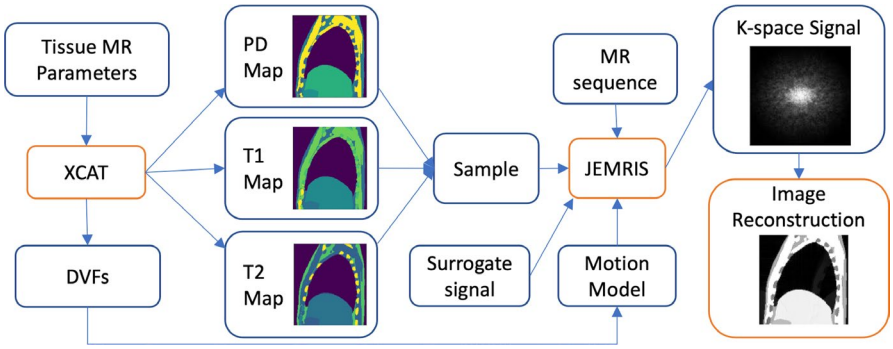


**FIGURE 1** Tissue MR properties and anatomical variables are passed into XCAT, which is used to generate proton density (PD), T1, and T2 maps of the tissues. These maps are packaged into a sample file, which is passed into our modified version of JEMRIS alongside the imaging sequence and our motion model. JEMRIS output gives the k-space signal, which can be used to reconstruct the MR image [Color figure can be viewed at wileyonlinelibrary.com]

these surfaces based on user-defined parameters, which specify body measurements, organ volumes and other variables. In our framework separate $T_1$, $T_2$ and proton density maps were generated. The corresponding values for each tissue were taken from Paganelli et al.[11] and the MRI Toolbox parameter database[12] and included in the parameter files (example parameter files are provided as supplementary files). $T_2$ values were substituted for $T_2$* as a complete set of data was not available. The generated maps were packaged into a JEMRIS sample file.

## 2.2 | Motion model

XCAT is also capable of simulating breathing motion based on respiratory mechanics and can be used to generate deformation vector fields (DVFs) of the phantom. Chest and diaphragm motion traces can be defined as inputs into the phantom, allowing for irregular and variable breathing motion which can include intracycle variation (hysteresis). The previous iteration of our framework used these DVFs for simulation. However the software generates full DVFs for each time point, which is inconvenient for storage, as simulating an average 4-min scan would require 400 frames. Furthermore, the DVFs output by the XCAT phantom directly may show inconsistent motion of adjacent structures.[13] Therefore, we created a motion model that describes the motion vector at each voxel based on the diaphragm/superior–inferior (SI) and chest/anterior–posterior (AP) signals, allowing full DVFs to be calculated based on a surrogate respiratory signal of arbitrary length and shape.

First, deformation vector fields were generated using XCAT. To correct errors where structures in the phantom move through each other, the XCAT DVFs were post-processed using the framework described by Eiben et al.[13] A linear motion model was then fitted to these DVFs using voxel-wise least-squares fitting using the original SI and AP signal values of the XCAT simulation.

Application of these two methods resulted in a motion model with three components in the form of vector fields. The first and second components describe the variation of the final DVF depending on the SI and AP signals, respectively, whereas the third component is a constant offset vector field. As a result, the predominant vector orientations found in the first two components are in the SI and AP direction, respectively. To model realistic breathing patterns within the framework, a surrogate motion signal giving SI and AP amplitudes is required. This can be acquired from a volunteer by tracking a specific point on the diaphragm (for SI) and the skin surface (for AP) in a two-dimensional (2D) cine sequence. These signals together with the components of the motion model can then be used to generate a time series of deformation fields X using for every timepoint t of the series:

$$\vec{X}(\vec{r},t) = \vec{C}_{AP}(\vec{r})s_{AP}(t) + \vec{C}_{SI}(\vec{r})s_{SI}(t) + \vec{C}_{O}(\vec{r}) \quad (1)$$

where $s_{AP/SI}$ is the surrogate signal and $C_{AP/SI/O}$ the vector fields. The components of the motion model can be used with different surrogate signals and only need to be regenerated when the anatomy of the phantom is changed.

## 2.3 | JEMRIS

The MR acquisition is simulated using our modified version of JEMRIS. The open-source MR simulator applies numerical solutions of Bloch equations to a system of spins. JEMRIS has the advantage of being extensible, allowing users to add features not present natively.[6] Within the software, the magnetic field is modeled as a function of time and position:

$$\vec{B}(\vec{r},t) = [\vec{G}(t)\cdot\vec{r}(t) + B_{NLG}(\vec{r},t) + \Delta B_0(\vec{r},t)\vec{e}_z + n = 1] \times N\sum(B^n_{1x}(\vec{r},t)\vec{e}_x + B^n_{1y}(\vec{r},t)\vec{e}_y) \quad (2)$$

To achieve motion, the position of a spin needs to be calculated as a function of time. The existing JEMRIS motion function moves the entire system of spins as one unit to achieve rigid motion. In the case of deformable motion different structures are moving in different directions simultaneously, therefore we have added a new trajectory function to JEMRIS, which calculates the position of each spin independently. To achieve this the simulator loads the motion model along with a surrogate signal at the start of each simulation, and then, for each time point of the time series calculates an updated spin position $r'$ according to $r'(t) = r + x(r,t)$, that is, substituting the original spin position $r$ with the one defined by the model displacement, $x$. These modified positions are used by the simulator to determine the magnetic field experienced by the spins due to gradients and calculate the signal received by coils. The motion model is spatially up-sampled using trilinear interpolation when defined at lower intrinsic resolution than the sample.

## 2.4 | Simulations

In order to demonstrate that the framework behaves as expected, acquisitions with two different sequences were simulated. To reduce the computation time of these initial simulations, a 2D sagittal slice through the lung was extracted from the XCAT phantoms instead of using the entire 3D volume. Nearest neighbor interpolation was used to increase the number of spins to run the simulations with various spin densities as required. If not enough spins are used for a simulation

phase cancellation artifacts can arise.[14] In our simulations, we assumed uniform coil sensitivity; however, JEMRIS does also have functionality for specifying custom coils.

The first sequence tested was a single-shot EPI with partial Fourier acquisition (65% asymmetric coverage). Partial Fourier was used to reduce the acquisition time and achieve a high framerate suitable for simulating a cine acquisition. For this simulation a surrogate breathing trace from a healthy volunteer was used (Figure 3c) with a phantom consisting of 540 × 540 spins 0.5 mm apart (31.6 spins per voxel). The parameters of the sequence were: TR = 100 ms, TE = 50 ms, FOV = 27 × 27 $cm^2$, flip angle 35°, voxel size 2.8 × 2.8 mm and phase encoding was applied in the AP direction. The simulation consisted of 180 cine frames, equivalent to 18 s of acquisition. For comparison, the same deformation fields were calculated outside the simulation framework and applied to an XCAT attenuation phantom using NiftyReg deformable image registration modules.[15]

In the second simulation, we wanted to create conditions where artifacts would arise. A spin echo sequence was used for all four simulations, with TR set to 2100 ms, simulating an interleaved multislice acquisition. Discrete ghost artifacts occur in the presence of periodic motion and the number of ghosts and their distance from each other depends on the duration of the motion period ($T$) relative to repetition time (TR). To demonstrate these effects, four different simulations with four different surrogate breathing traces were used. The first trace was based on a mathematical model of diaphragm motion[16] with $T$ = 4.2 s. (Figure 3a). For the second simulation, we shifted the first trace by one second (Figure 3b). For the third simulation, we used a trace recorded from a healthy volunteer and chose a single respiratory cycle with $T$ = 3 s that was repeated for the duration of the acquisition for consistent amplitude and respiratory cycle length (Figure 3c). The fourth simulation was carried out with an unmodified trace acquired from a healthy volunteer that had varying amplitude and respiratory cycle length (Figure 3d). The other parameters of the sequence were: TE = 5 ms, FOV = 26 × 32 $cm^2$, voxel size 2.7 × 2.7 mm, and phase encoding was in AP direction. For this simulation, a phantom of 520 x 640 spins was used with the spins spaced 0.5 mm apart (28.9 spins per voxel).

## 3 | RESULTS

### 3.1 | Single-shot EPI (Cine) simulations

Figure 2 shows a number of still frames from the cine simulation. Movement of the chest wall along the AP axis and movement of the abdominal organs along the SI axis is visible and shows good agreement with the corresponding frames from the original deformations applied to the source image. The full simulated cine is included as a supplementary video. In the video, it can be seen that each of the respiratory cycles differs slightly from the previous one, corresponding to the surrogate signal used. The partial Fourier acquisition introduced a reflection of the chest wall due to differences of $T_2^*$ decay over the sampled and synthesized k-space.

### 3.2 | TSE simulations

The simulations of the TSE sequence aimed to create conditions where motion artifacts are known to be present. Figure 3a shows no ghosts, as the sequence repetition occurs at the same respiratory phase each time. A single discrete ghost, shifted by half of the image in the phase encode direction (AP), is present in Figure 3b, as the sequence repetition time is exactly half of the motion period. In this simulation, all instances of the sequence repetition aligned with either the end exhale or end inhale phase, creating two superimposed images of the diaphragm at different positions. Figure 3c shows multiple ghosts. In this simulation, the motion was periodic, but repetition time of the sequence was longer than half of the motion period (2100 and 1500 ms, respectively), causing the ghosts to be more closely spaced. Figure 3d shows diffuse noise in the phase-encoding (AP) direction and no discrete ghosts. This is expected, because the respiratory motion in this simulation was not periodic. Therefore, these results align well with the behavior previously described in the literature.[17]

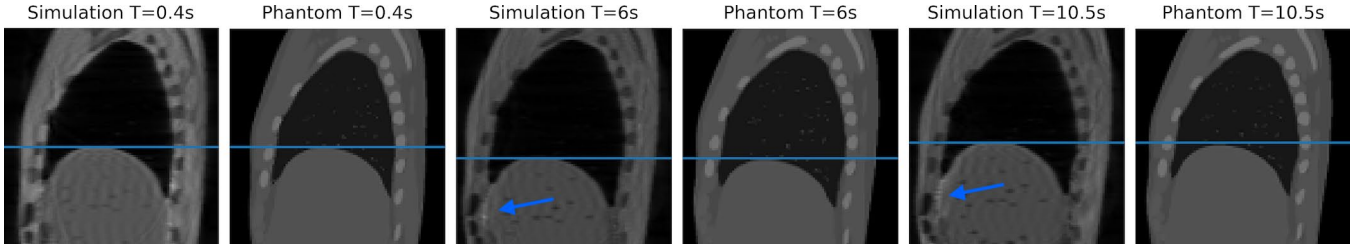


**FIGURE 2** Frames from the cine acquisition compared to corresponding deformations applied to source image. Arrows indicate areas with inaccuracies in the presentation of sliding motion [Color figure can be viewed at wileyonlinelibrary.com]

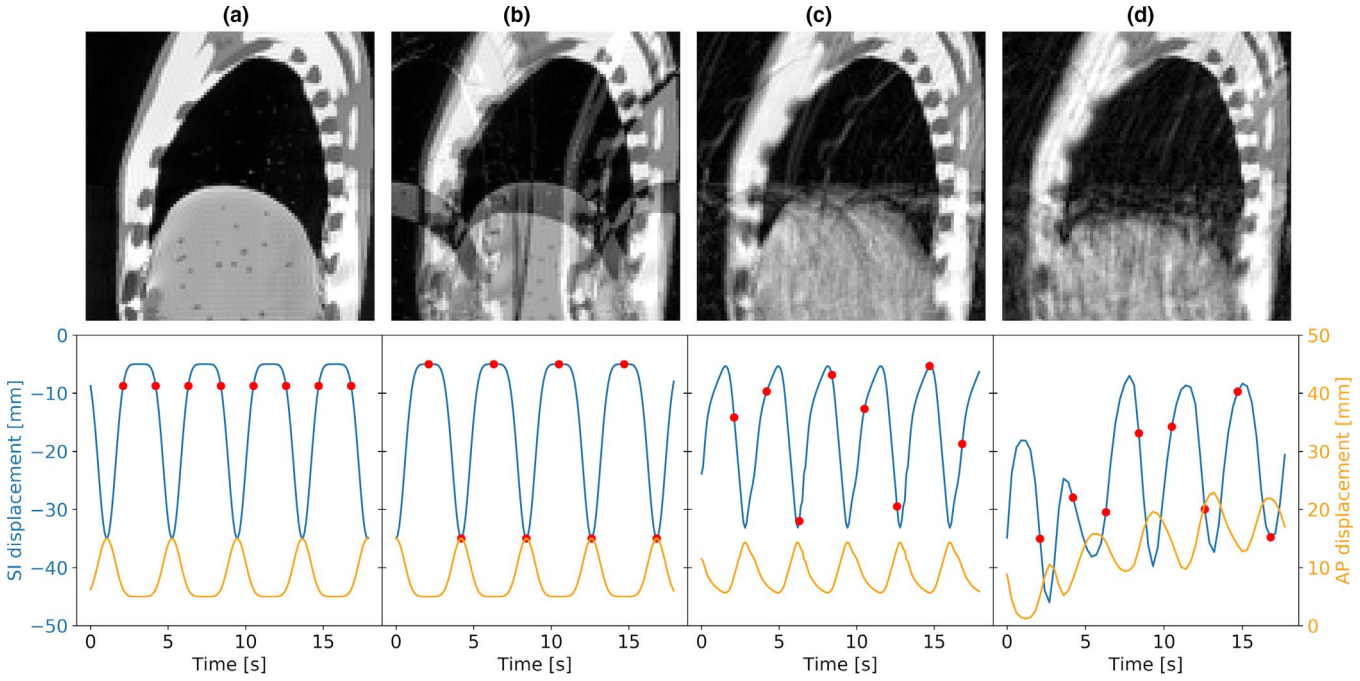


**FIGURE 3** TSE simulations with corresponding surrogate traces. Red points indicate sequence repetition times. (a) Simulation with a trace based on a mathematical model of diaphragm motion. (b) Simulation with the trace from A shifted by one second. (c) Simulation with single repeating respiratory cycle from a healthy volunteer. (d) Simulation with a trace recorded from a healthy volunteer [Color figure can be viewed at wileyonlinelibrary.com]

### 3.3 | Computation time

To assess the average run time on our test machine (running at 2.2 GHz with a single core), we repeated each simulation five times and calculated the average. The 2D TSE sequence required around 12 h of computation time with 197 361 spins. However, JEMRIS supports parallel computation using MPI so by using 20 cores with 40 threads for processing the actual wall time for simulation was around 18 min. Compared to simulations with no motion and rigid motion, respiratory motion increases simulation time by 3.8% and 0.1% respectively. The 2D cine sequence with 203 206 spins required 246 h computation time (6.3 h wall time). For this sequence, respiratory motion increases simulation time by 2.4% compared to no motion and decreases simulation time by 1% compared to rigid motion.

## 4 | DISCUSSION

### 4.1 | Existing MRI simulators

We developed a digital phantom framework, which is anatomically accurate, incorporates realistic breathing patterns and can simulate deformable motion. Recently, two other XCAT-based MR simulation frameworks have been presented in literature: MRXCAT[18] and CoMBAT,[11] both based on analytical models. The benefit of these models is that the simulations are not computationally demanding, although not all MR phenomena can be described analytically. When developing a new MR sequence, one of the main considerations is whether any artifacts are produced. As MR images are acquired in the frequency domain, the source of an artifact may not be immediately obvious. Bloch simulation has the advantage of being able to disable certain phenomena to understand their impact on the image.

In analytical models, MR signal intensities are assigned to the entire XCAT map at once, and then the simulated *k*-space is sampled according to the sequence trajectory. Therefore, these frameworks assume acquisition of the entire *k*-space is instantaneous while in reality *k*-space is sampled point by point. Movement during sampling leads to inconsistencies in spatial encoding, creating artifacts such as ones seen in the TSE simulations in this paper. $T_2^*$ effects are not accounted for in the two analytical models. While simulations presented in this paper have estimated $T_2^*$ to be equal to $T_2$, the effect is still visible in the cine simulation as a chest wall reflection. For a more accurate presentation of the $T_2^*$ effects, the missing values must be measured with in vivo experiments.

### 4.2 | Motion model

Using the motion model gives the framework additional flexibility, as the breathing pattern can be changed by

using a different surrogate signal, allowing the user to match the conditions of the simulation more closely to those of the clinical scenario. For example, it is possible to simulate various levels of breath-hold or respiratory pattern drift during radiotherapy. In the previous version of this framework, the full deformation fields for each time point were calculated prior to simulation and contained in a single file, meaning that for longer simulations large amounts of data had to be stored in memory. The current version is much more efficient in that regard as only three vector fields are required for any simulation. For comparison, the new motion model file with 16 min of data is 1521 KB, while the old model with the same amount of data would have been 450MB. It should be noted that both of these files only contain a single 2D slice extracted from the full 3D motion model. For 3D simulations, the file size would increase considerably. The new motion model is also more efficient in terms of computation time. With the previous motion model the DVF had to be interpolated for every spin at every time point. As $C_{AP/SI/O}$ in Equation 1 do not vary with time, the new motion model allows for the interpolation step to be completed once for every spin. Calculation of the spin position at any time is then just a matter of a linear combination of these three vectors and extremely efficient. This is demonstrated by a reduction of computation time compared to rigid motion in the cine experiment.

When choosing a breathing trace for simulations, it is important to consider how the respiratory phases in the surrogate signal correspond to sequence sampling times. Figure 3 shows two simulations with the same breathing trace (A and B), shifted by one second. In the first simulation the phantom is in the same respiratory phase at each sampling point and no artifacts are formed. However, in the second simulation, the sampling alternates between end exhalation and end inhalation, creating a discrete ghost. Therefore, the timing of the surrogate signal can affect the outcome of the simulation. Synthetic signals are useful for understanding how certain aspects of respiratory motion affect a sequence, as all variables can be accurately controlled. In reality, both these simulations are too perfect and more realistic results can be achieved with a real recorded surrogate signal. If no recorded signal is available, the synthetic signals could be modified to have variation in both amplitude and period to achieve a more realistic result. These variations have been quantified by Rit et al.[19]

## 4.3 | Remaining limitations

One major source of artifacts is object-induced distortions in $B_0$, which is not included in our framework. Calculations in JEMRIS include the $B_0$ term (see Equation 2); however, the software does not calculate this term dynamically. Therefore to include these effects in simulations, additional modification of JEMRIS will be required. One current limitation of the motion model is that it cannot represent sliding motion which can lead to inaccuracies at sliding boundaries such as between the lungs and chest wall. The effects of this are visible in Figure 2. There is ongoing work to extend the motion models so that they can model sliding motion more accurately, and in the future this will be incorporated into our simulations. Additionally, the current motion model does not include cardiac motion and further work would be required to implement this.

All computation for this study was done using a 2D plane of spins to reduce the computational burden, but this means that some behaviors are not accurately simulated, for example, we lack through-plane motion or slice selective excitation. Here we deliberately selected an imaging slice where the motion is almost entirely within the plane, avoiding the need to simulate these effects. The framework does support 3D samples and motion, as well as arbitrary gradient and RF waveforms, but these all come at a cost in simulation time. From our tests, using slice selective pulses in the TSE sequence increased the simulation time per spin by a factor of 2, while also requiring many more spins to accurately describe the system. However, as demonstrated by Stöcker et al. in the original JEMRIS paper,[6] simulations parallelize extremely well, so calculation time can be arbitrarily reduced by increasing the number of available cores.

## 4.4 | Applications

We will use this framework to develop sequences for MR-guided lung radiotherapy, to achieve shorter acquisition times while maintaining acceptable image quality and spatial accuracy. The application of MR imaging to image guided radiotherapy has different requirements than in radiology. With our simulator, we can generate images at different reduced acquisition times and quantify if these are still suitable for purpose. To enable other groups developing novel MR imaging sequences to make use of this method our modifications to JEMRIS have been incorporated into the main source code. Please refer to the appendix for links to repositories containing the phantom files and instructions for use. In the example, images we focused on the thoracic region and respiratory motion; however, the framework has capability of generating phantoms of any part of the body. Similarly to lung cancer, tumors in abdominal organs are difficult to treat with radiotherapy due to the presence of respiratory motion and we foresee wide applications to optimize sequences for this region.

## 5 | CONCLUSION

We present a deformable 4D digital phantom framework for MR sequence development. The framework incorporates anatomical structure, realistic breathing patterns, deformable motion, and Bloch simulation to achieve accurate simulation of MRI. The performance of the framework is demonstrated through generating a lung model with respiratory motion and imaging multiple respiratory cycles with a cine sequence and demonstrating the expected motion ghosts from a T2-weighted spin echo acquisition.

## ACKNOWLEDGMENTS

This work was supported by the Engineering and Physical Sciences Research Council (grant number EP/R5131631/1). Marcel van Herk was supported by NIHR Manchester Biomedical Research Centre. Jamie McClelland and Björn Eiben are supported by a Cancer Research UK NetworkAccelerator Award grant (A21993).

## CONFLICTS OF INTEREST

None.

## DATA AVAILABILITY STATEMENT

The data that support the findings of this study are openly available in Github at https://github.com/hmhanson/4DPhantomMRI and https://github.com/UCL/motionModelFromXCATDVFs.

## REFERENCES

1. Bray F, Ferlay J, Soerjomataram I, Siegel RL, Torre LA, Jemal A. Global cancer statistics 2018: GLOBOCAN estimates of incidence and mortality worldwide for 36 cancers in 185 countries. *CA Cancer J Clin*. 2018;68(6):394-424. https://doi.org/10.3322/caac.21492
2. Finazzi T, Palacios MA, Spoelstra FOB, et al. Role of on-table plan adaptation in MR-guided ablative radiation therapy for central lung tumors. *Int J Radiat Oncol Biol Phys*. 2019;104(4):933-941. https://doi.org/10.1016/j.ijrobp.2019.03.035
3. Finazzi T, van Sörnsen de Koste JR, Palacios MA, et al. Delivery of magnetic resonance-guided single-fraction stereotactic lung radiotherapy. *Phys Imaging Radiat Oncol*. 2020;14:17-23. https://doi.org/10.1016/j.phro.2020.05.002
4. Johnson-Hart CN, Price GJ, Faivre-Finn C, Aznar MC, van Herk M. Residual setup errors towards the heart after image guidance linked with poorer survival in lung cancer patients: do we need stricter IGRT protocols? *Int J Radiat Oncol Biol Phys*. 2018;102(2):434-442. https://doi.org/10.1016/j.ijrobp.2018.05.052
5. Johnson-Hart C, Price G, Vasquez Osorio E, Faivre-Finn C, van Herk M. The impact of baseline shifts towards the heart after image guidance on survival in lung SABR patients. *Radiother Oncol*. Published online November 15, 2019. https://doi.org/10.1016/j.radonc.2019.10.018
6. Stöcker T, Vahedipour K, Pflugfelder D, Shah NJ. High-performance computing MRI simulations. *Magn Reson Med*. 2010;64(1):186-193. https://doi.org/10.1002/mrm.22406
7. Benoit-Cattin H, Collewet G, Belaroussi B, Saint-Jalmes H, Odet C. The SIMRI project: a versatile and interactive MRI simulator. *J Magn Reson*. 2005;173(1):97-115. https://doi.org/10.1016/j.jmr.2004.09.027
8. Yoder DA, Zhao Y, Paschal CB, Fitzpatrick JM. MRI simulator with object-specific field map calculations. *Magn Reson Imaging*. 2004;22(3):315-328. https://doi.org/10.1016/j.mri.2003.10.001
9. Segars WP, Sturgeon G, Mendonca S, Grimes J, Tsui BMW. 4D XCAT phantom for multimodality imaging research. *Med Phys*. 2010;37(9):4902-4915. https://doi.org/10.1118/1.3480985
10. Hanson HM, van Herk M, Cobben D, Rowland BC. 4D deformable digital phantom for MRI sequence development. In: Proceedings of the International Society for Magnetic Resonance in Medicine 28; 2020.
11. Paganelli C, Summers P, Gianoli C, Bellomi M, Baroni G, Riboldi M. A tool for validating MRI-guided strategies: a digital breathing CT/MRI phantom of the abdominal site. *Med Biol Eng Comput*. 2017;55(11):2001-2014. https://doi.org/10.1007/s11517-017-1646-6
12. McMillan A. MRI toolbox - parameter database. Updated 2013. Accessed October 9, 2019. http://www.mritoolbox.com/ParameterDatabase.html
13. Eiben B, Bertholet J, Menten MJ, Nill S, Oelfke U, McClelland JR. Consistent and invertible deformation vector fields for a breathing anthropomorphic phantom: a post-processing framework for the XCAT phantom. *Phys Med Biol*. 2020;65(16): 165005. https://doi.org/10.1088/1361-6560/ab8533
14. Kwan RK-S, Evans AC, Pike GB. MRI simulation-based evaluation of image-processing and classification methods. *IEEE Trans Med Imaging*. 1999;18(11):1085-1097. https://doi.org/10.1109/42.816072
15. Modat M, Ridgway GR, Taylor ZA, et al. Fast free-form deformation using graphics processing units. *Comput Methods Programs Biomed*. 2010;98(3):278-284. https://doi.org/10.1016/j.cmpb.2009.09.002
16. Lujan AE, Larsen EW, Balter JM, Haken RKT. A method for incorporating organ motion due to breathing into 3D dose calculations. *Med Phys*. 1999;26(5):7.
17. Zaitsev M, Maclaren J, Herbst M. Motion artifacts in MRI: A complex problem with many partial solutions: Motion Artifacts and Correction. *J Magn Reson Imaging*. 2015;42(4):887-901. https://doi.org/10.1002/jmri.24850
18. Wissmann L, Santelli C, Segars WP, Kozerke SMRXCAT. Realistic numerical phantoms for cardiovascular magnetic resonance. *J Cardiovasc Magn Reson*. 2014;16(1): https://doi.org/10.1186/s12968-014-0063-3
19. Rit S, van Herk M, Zijp L, Sonke J-J. Quantification of the variability of diaphragm motion and implications for treatment margin construction. *Int J Radiat Oncol Biol Phys*. 2012;82(3):e399-e407. https://doi.org/10.1016/j.ijrobp.2011.06.1986

## SUPPORTING INFORMATION

Additional supporting information may be found online in the Supporting Information section.

**How to cite this article:** Hanson HM, Eiben B, McClelland JR, van Herk M, Rowland BC. Technical Note: Four-dimensional deformable digital phantom for MRI sequence development. *Med. Phys*. 2021;48:5406–5413. https://doi.org/10.1002/mp.15036

## APPENDIX

### CINE SIMULATION

The supplemental video shows the full cine simulation.

### PHANTOM FILES

All phantom files and instructions for use are available at https://github.com/hmhanson/4DPhantomMRI.

### MOTION MODEL FILES

All motion model component files are available at https://github.com/UCL/motionModelFromXCATDVFs.